Moist Convection and the Vertical Structure and Water Abundance of Jupiter's Atmosphere

ANTHONY D. DEL GENIO

NASA/Goddard Institute for Space Studies, New York, New York 10025

AND

KEVIN B. McGRATTAN[1]

Centel Federal Services Corporation, Institute for Space Studies, New York, New York 10025

We explore the consequences of moist convection on Jupiter with a one-dimensional version of the cumulus parameterization used in the GISS general circulation model. The model predicts the collective effects of an ensemble of moist convective plumes on a conditionally unstable atmosphere. Heating/cooling and drying/moistening of the large-scale environment occur through compensating subsidence, detrainment of updraft air at cloud top, and evaporation and melting of falling condensate. Dry convective adjustment and stratiform cloud formation are included to remove superadiabatic lapse rates and supersaturated humidities, respectively. The model also transports parahydrogen fraction as a passive tracer. We make two different assumptions about how convection operates on Jupiter. In the first scenario we assume that convection dominates all other processes, modifying an initial temperature and moisture profile until it reaches neutral stability. Three regimes are possible: Pure moist convective, mixed moist–dry convective, and primarily dry convective. The outcome depends on the assumed deep water abundance, efficiency of condensate evaporation, and initial temperature profile. Relative humidity just below cloud top is low in the moist convective regime but increases steadily with depth. Isolated dry convection layers in the mixed regime produce sharp vertical variations of relative humidity and multiple water cloud layers. In all cases, severe water depletion is possible only over a narrow range of altitudes. In particular, the water vapor profile inferred by Bjoraker *et al.* (1986, *Astrophys. J.* **311**, 1058–1072) cannot be reconciled with the effects of moist convection, regardless of whether the deep abundance is subsolar, solar, or supersolar. Significant cloud-base stable layers a scale height or less in depth form when condensate evaporation and dry convection are important, but the degree of stabilization is always considerably less than the theoretical limit. Convective transports produce subequilibrium parahydrogen fractions and small or negative gradients near the visible cloud level. We also examine the alternative assumption that a quasiequilibrium prevails between moist convection and other processes on Jupiter. In this scenario we calculate the cumulus mass flux consistent with the Jovian internal heat flux and diagnose the large-scale vertical advection required to balance the convective heating. The equilibrium configuration for near-neutral static stability is a series of thin convection layers capped by thin cloud layers and a "staircase" vertical profile of temperature, humidity, and parahydrogen fraction. © 1990 Academic Press, Inc.

---

[1] Present affiliation: Courant Institute of Mathematical Sciences, New York University, New York, NY 10012.

1. INTRODUCTION

Moist convection is a pervasive influence on the structure and dynamics of Earth's atmosphere. It controls the lapse rate in the tropical troposphere, largely drives the Hadley and Walker circulations, and forces a variety of wave motions and other circulations on many scales. It acts as the agent of coupling between the atmosphere and ocean and thereby determines much of the interannual variability of Earth's climate. Moist convection redistributes water vapor vertically, controlling the humidity profile at low latitudes and contributing to Earth's multilayered cloud structure. Changes in moist convection strength as trace gas concentrations increase on Earth and the resulting water vapor and cloud feedbacks affect estimates of future global warming.

The atmosphere of Jupiter contains a variety of condensible species (Weidenschilling and Lewis 1973), thus raising the possibility that moist convection is a critical process there as well. To date, relatively little attention has been focused on moist processes in Jovian atmospheres, primarily because of the complexity of cloud/convection physics and uncertainties in the abundances of condensible gases. However, several workers have suggested that latent heat release and molecular weight differentiation may be important controls on the dynamics near and below the visible cloud level. For a solar composition atmosphere, water is the most important potential condensate, producing maximum buoyancy contrasts equivalent to a few degrees in temperature. On the basis of these considerations, it has been proposed that water condensation drives meridional circulations which account for Jupiter's belts and zones (Barcilon and Gierasch 1970, Gierasch 1976) and creates a stable trapping layer consistent with the propagation characteristics of observed equatorial waves (Allison 1990). Ingersoll (1976) and Gierasch and Conrath (1985, 1987) discuss phase change effects on dynamics and vertical structure in a broader context.

In recent years, the penetrative nature of moist convection has been recognized, leading to several assessments of the characteristics of cumulus clouds in a given Jovian environment and the effect of these clouds in turn on the environment. Stoker (1986) used the traditional entraining plume model from terrestrial meteorology to estimate updraft speeds and cloud top heights for cumulus clouds on Jupiter. Lunine and Hunten (1987) hypothesized that subsidence of the relatively cloud-free environment between cumulus clouds might cause substantial drying and subsaturation of water vapor on large scales, despite a deep solar abundance. This suggestion was a response to the surprising results of an analysis of airborne and Voyager IRIS spectra of Jupiter by Bjoraker et al. (1986). (See also Lellouch et al. 1989 and the discussion in Section 5a.) Bjoraker et al. infer water vapor mixing ratios that are depleted by approximately a factor of 50 relative to a solar abundance in the 2- to 6-bar region of Jupiter. If these values are indicative of the deep abundance of oxygen on Jupiter, condensation effects cannot play an important role in the dynamics. Consistency with studies of the equilibrium chemistry of Jupiter is also a problem (Carlson et al. 1987, Fegley and Prinn 1988). A plausible explanation for how Jupiter might have evolved into a state with such severe global depletion of oxygen has not yet been advanced. It is therefore crucial to quantitatively evaluate the viability of Lunine and Hunten's suggestion, which offers a possible way to reconcile local water depletion with global solar abundance.

The cumulus parameterizations used in general circulation models (GCMs) are well suited to address such questions. Unlike the work of Stoker (1986), which applies to thermodynamic conditions within individual clouds themselves, cumulus parameterizations seek to determine the collective effect of an ensemble of cumulus clouds on the surrounding large-scale environment. If the fractional area covered by active cumulus clouds is small, then it is the larger be-

tween-cloud area which determines the style of large-scale dynamics and contributes most to remote sensing observations. On Earth, active cumulus occupy only a few percent of the globe, even in the Intertropical Convergence Zone (Riehl and Malkus 1958, Fu *et al.* 1990). Lunine and Hunten (1987) apply mixing length arguments to suggest that the same is true for Jupiter.

Early versions of terrestrial GCMs bypassed the physics of moist convection by using a moist adiabatic adjustment (Manabe *et al.* 1965). This scheme assumes that moist convection occurs whenever the atmosphere is saturated (or supersaturated) and conditionally unstable (i.e., the lapse rate lies between the moist and dry adiabats); it simply adjusts the atmosphere back to a saturated moist adiabat. This does not accurately reflect conditions outside the clouds, where the atmosphere often remains unsaturated and conditionally unstable in the presence of convection (Frank 1983).

Arakawa and Schubert (1974) and others have presented a different picture of the effect of moist convection on the environment. In their view latent heat release within cumulus clouds does not directly warm the environment—it serves merely to maintain the buoyancy of a rising cloudy parcel of air. Mixing of cloud properties with the environment occurs only at cloud top, near where the parcel buoyancy vanishes. Heating of the environment occurs primarily indirectly via adiabatic warming due to large-scale compensating subsidence. The penetrative convection view of cumulus parameterization has been verified by terrestrial field studies (cf. Arakawa and Chen 1987).

Considerable uncertainty remains today in the detailed modeling of moist convection as it applies to climate change simulations (where cloud cover changes of order $\pm 1\%$ must be predicted) or latent heat feedbacks on dynamics (where the small difference between convective heating and adiabatic cooling is important). However, the

basic features of moist convection are understood well enough to enable GCMs to simulate the first-order structure and circulation of the present terrestrial atmosphere. A study of convective influences with a penetrative cumulus parameterization can therefore be expected to provide reasonable answers to order-of-magnitude questions about Jupiter's vertical structure. We caution the reader, though, to remember that no direct, unambiguous observations of water condensation processes below the visible cloud level on Jupiter presently exist to validate our approach.

In this paper we apply the GISS GCM cumulus parameterization in one dimension to investigate the effects of moist convection on the large-scale structure of the Jupiter atmosphere. We address the following questions: Is there a value of the deep abundance of water for which the effects of moist convection can produce the vertical humidity profile retrieved by Bjoraker *et al.* (1986)? Under what conditions does moist convection give rise to a deep stable layer? What is the strength and vertical extent of such a layer when it exists? Are there any visible cloud level diagnostics of cumulus activity? What is the relationship between moist convection and other dynamical processes on Jupiter? In Section 2 we describe basic cumulus thermodynamics and our parameterization of convective processes. Section 3 explores the nature of the neutrally stable state produced by moist convection in the absence of other physical processes. In Section 4 we investigate the possible consequences of a quasiequilibrium between moist convection, the Jovian internal heat flux, and large-scale motions. We discuss the implications of our results in Section 5.

2. CUMULUS THERMODYNAMICS AND PARAMETERIZATION

The processes included in our cumulus parameterization are indicated schematically in Fig. 1. We begin by defining the dry static energy (s) and moist static energy (h) of a parcel of air per unit mass (units of J
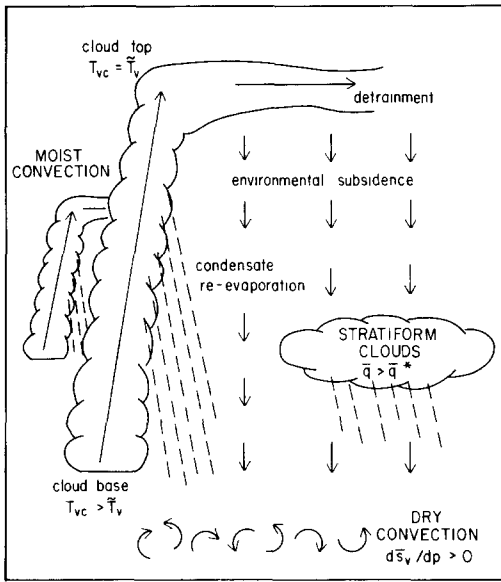
FIG 1. A schematic diagram of processes included in the one-dimensional cumulus parameterization.

kg^{-1}) as

$$s = c_pT + gz \qquad (1)$$

$$h = c_pT + gz + Lq, \qquad (2)$$

where c_p is the specific heat at constant pressure, T the temperature, g the acceleration due to gravity, z the altitude, L the latent heat of condensation, and q the mass of condensible vapor per unit total mass of atmosphere (called the specific humidity). It is easily shown that s is conserved in dry adiabatic ascent and that h is approximately conserved in moist adiabatic ascent. Thus, s and h are analogous to potential temperature and equivalent potential temperature, respectively.

A parcel of moist but unsaturated air, if displaced, conserves s until reaching its lifting condensation level (LCL), at which point it becomes saturated and a cloud forms. Further displacement without dilution conserves h instead. In a conditionally unstable atmosphere, the parcel is negatively buoyant during its initial ascent. Lifting beyond the LCL, however, may bring the parcel to its level of free convection

(LFC), at which point it becomes positively buoyant with respect to its surrounding environment. There are three contributors to the density difference between the parcel and its environment: Temperature (warmer air is more buoyant), molecular weight (air composed of lighter molecules is more buoyant), and condensate content (air with less condensed substance is more buoyant). The net effect of these competing influences on buoyancy is embodied in the virtual temperature T_v (cf. Saunders 1957), defined by

$$T_v = T \frac{(1 + \chi/\varepsilon)}{(1 + \chi)} (1 - l), \qquad (3)$$

where χ is the condensible vapor mass per unit mass of noncondensible gases (called the vapor mass mixing ratio), l the condensate mass mixing ratio, and $\varepsilon = m_v/m_d$ the ratio of the molecular weights of the vapor and dry air. Note that $q = \chi/(1 + \chi) \cong \chi$ if $\chi \ll 1$ and that the H_2O mole fraction relative to H_2 is χ/ε divided by the abundance of H_2. If the parcel's T_v exceeds that of the environment, it is buoyant and convectively unstable.

For $\chi \ll 1$, (3) can be expressed approximately as

$$T_v \cong T \left[1 + \left(\frac{1}{\varepsilon} - 1 \right) \chi - l \right]. \qquad (4)$$

On Earth, where water is lighter than dry air ($\varepsilon < 1$), molecular weight differences between a moist parcel and the drier environment act in the same sense as temperature differences and are secondary in importance. On Jupiter, though, $\varepsilon > 1$ because dry Jovian "air" is an H_2–He mixture. Thus, molecular weight differentiation opposes thermal effects on buoyancy on Jupiter; this leads to some extremely interesting behavior, as we will see in the following sections. Condensate loading is always a negative influence on buoyancy but is quite difficult to estimate because of the complexity of cloud microphysics.

The concept of cumulus parameteriza-

tion can be summarized as follows. Given an atmospheric column with known instantaneous vertical profiles of temperature and moisture (and therefore s and q) averaged over a horizontal scale much larger than that of an individual cloud, how will the action of cumulus convection modify these profiles as a function of time? The procedure involves five steps: (i) Diagnosis of whether the vertical structure of s and q is unstable to moist convection at a particular level; (ii) Determination of the total mass per unit time rising from cloud base in cumulus updrafts; (iii) Estimation of the eventual cloud-top height; (iv) Computation of the response of the environment to the convection; (v) Partitioning of the condensed water into a part which leaves the system through the lower boundary as precipitation and a part which melts and/or evaporates into the subsaturated environment as it falls.

If our model atmosphere is divided into a number of layers, we can diagnose the onset of moist convection at a given level by adiabatically lifting a parcel of air with the properties of the environment at that level to the next highest layer, testing to see whether it becomes saturated (i.e., whether it reaches its LCL), and if so, testing to see whether $T_{vc} > \bar{T}_v$, where ( )$_c$ denotes the cloud parcel and (¯) the cloud-free environment. If this instability criterion is satisfied, the parcel has reached its LFC and moist convection occurs.

The next step is to calculate the rate at which mass rises per unit area from cloud base in the ensemble of cumulus updrafts. The GISS GCM gives a satisfactory overall simulation of Earth's climate even with a fixed, arbitrary choice for the cumulus mass flux (Hansen et al. 1983) and a very good simulation with a physically based, interactive estimate of this quantity (Del Genio and Yao 1988, Yao and Del Genio 1989). In Sections 3 and 4 we describe two different approaches to this problem.

We then consider the question of cloud-top height, which determines the altitude range over which the atmosphere is affected by convection. Having become buoyant by being lifted one layer, the parcel continues to rise moist adiabatically to the next level and is tested again. If it is still buoyant, the cloudy parcel proceeds to higher and higher levels until its buoyancy vanishes, i.e., it reaches a level at which $T_{vc} \leq \bar{T}_v$. This defines the cloud top. (Actually, parcels of air in real cumulus clouds slightly overshoot the level of vanishing buoyancy and then oscillate about this level until damped by mixing with the environment (Knupp and Cotton 1985). This can be important for the injection of trace gases into the upper atmosphere but is irrelevant for computing effects on the bulk of the troposphere, which is our concern here.) In true moist adiabatic ascent, condensate is transported upward in the cloud parcel with no precipitation. In our computations, we assume pseudoadiabatic ascent: All condensed water is left behind at the level at which it condenses. This maximizes cloud-top height (by eliminating negative buoyancy due to condensate loading) and minimizes the ability of condensate reevaporation to moisten the environment above cloud base (by transporting none of the condensate to the drier upper levels). Efficient rainout is consistent with microphysical analyses of the Jovian water clouds (cf. Fig. 3 of Carlson et al. 1988) and is precisely the situation envisioned by Lunine and Hunten (1987).

The effect that moist convection has on the environment (i.e., the time rate of change of s and q) is most easily seen by considering the thermodynamic energy equation. Let (¯) denote the large-scale average over an area which includes the ensemble of cumulus clouds and the environment affected by the clouds (e.g., the area of a gridbox in a GCM application of the scheme). Let ( )′ denote subgrid-scale fluctuations about this large-scale mean due to convection; all other eddies are neglected. If horizontal transports are ignored, then in

pressure coordinates,

$$\frac{\partial \bar{s}}{\partial t} + \bar{\omega} \frac{\partial \bar{s}}{\partial p} = -\frac{\partial}{\partial p} (\overline{\omega' s'})$$
$$+ L(\bar{C} - \bar{E}) + Q_R, \quad (5)$$

where t is time, p is pressure, $\omega = dp/dt$ is the vertical velocity in pressure coordinates, $\bar{C}$ and $\bar{E}$ are the net condensation and evaporation rates, respectively, and Q_R is the radiative heating. Our goal is to specify all the terms in (5) so that $\partial \bar{s}/\partial t$ can be calculated.

The cumulus clouds are assumed to cover a fractional area $\sigma \ll 1$. Since cloud-environment temperature differences are small,

$$\bar{s} = \sigma s_c + (1 - \sigma)\tilde{s} \cong \tilde{s}. \quad (6)$$

Cloud vertical velocities, however, may greatly exceed those elsewhere; we simply write

$$\bar{\omega} = \sigma \omega_c + (1 - \sigma)\tilde{\omega} = M_c + \tilde{M}, \quad (7)$$

where M_c and $\tilde{M}$ are called the cumulus mass flux and environmental mass flux, respectively. The dimension of $\bar{\omega}$, M_c and $\tilde{M}$ in p-coordinates is mb h^{-1}; to convert these terms to actual mass flux units in z-coordinates, (7) should be divided by g. In general, $\bar{\omega} \neq 0$ over the altitude range of a cumulus cloud. In a Hadley cell, for example, $\bar{\omega} < 0$ in the rising branch and >0 in the sinking branch. However, in the simple case that $\bar{\omega} = 0$, $\tilde{M} = -M_c$, i.e., the cumulus mass flux is balanced by compensating environmental subsidence.

It is straightforward to show (Arakawa and Schubert 1974) that to $O(\sigma)$,

$$\overline{\omega' s'} \cong M_c(s_c - \bar{s}). \quad (8)$$

Then if $Q_R = 0$,

$$\frac{\partial \bar{s}}{\partial t} \cong -\bar{\omega} \frac{\partial \bar{s}}{\partial p} - \frac{\partial}{\partial p} [M_c(s_c - \bar{s})]$$
$$+ L(\bar{C} - \bar{E})$$
$$= -\tilde{M} \frac{\partial \bar{s}}{\partial p} - M_c \frac{\partial s_c}{\partial p} + L\bar{C}$$
$$- (s_c - \bar{s}) \frac{\partial M_c}{\partial p} - L\bar{E}, \quad (9)$$

using (7). M_c can vary with height if environmental air is entrained into the clouds. This effect is included in the operational GISS parameterization (Yao and Del Genio 1989), but we ignore it here for simplicity because vigorous deep cumulus have small entrainment rates. Our clouds are thus comparable to the low entrainment cases of Stoker (1986). The impact of entrainment would be to slightly lower cloud tops with little effect at lower altitudes.

With this simplification, $\partial M_c/\partial p = 0$ except at cloud top ($p = p_t$), where the cumulus mass flux converges over a distance taken to be the thickness of the cloud top layer Δp. The divergence of M_c at cloud base ($p = p_b$) does not contribute to $\partial \bar{s}/\partial t$ because $s_c = \bar{s}$ there. Within the ascending cloud itself, h_c is conserved but s_c is not because of latent heat release, i.e.,

$$M_c \frac{\partial s_c}{\partial p} = -LM_c \frac{\partial q_c}{\partial p} = L\bar{C}, \quad (10)$$

where $q_c(p)$ is the saturated value $q^*(T_c, p)$ given by the Clausius–Clapeyron equation. Using (10), we can thus rewrite (9) in the form

$$\frac{\partial \bar{s}}{\partial t} \cong -\tilde{M} \frac{\partial \bar{s}}{\partial p}$$
$$- (s_c - \bar{s}) \frac{M_c}{\Delta p} \delta(p - p_t) - L\bar{E}. \quad (11)$$

In (11), $\bar{s}(p)$ is the given initial thermal structure, s_c is determined by the moist adiabatic lapse rate according to (10), p_t is determined by the vanishing buoyancy criterion, M_c is calculated as discussed in Sections 3 and 4, and $\tilde{M}$ is given by (7) after either calculating the large-scale vertical motion (as in a GCM) or prescribing it. We describe the computation of $\bar{E}$ below.

A similar equation can be derived for moisture changes. Care must be taken in making the equivalent approximation to (6) because $q_c = q^*(T_c, p)$ can be much greater than $\bar{q}$ if environmental relative humidity is low. In our calculations $\sigma \ll 10^{-2}$ and $\bar{q}/q_c \gtrsim 10^{-2}$ at all times, so we can safely assume

that $\bar{q} \cong \tilde{q}$. Using the moisture continuity equation and proceeding as we did for s, we can then show that

$$\frac{\partial \bar{q}}{\partial t} \cong -\tilde{M} \frac{\partial \bar{q}}{\partial p}$$

$$- (q_c - \bar{q}) \frac{M_c}{\Delta p} \delta(p - p_t) + \bar{E}. \quad (12)$$

(11) and (12) clearly illustrate the effects of moist convection on the large-scale environment. The first term on the right-hand-sides of (11) and (12) represents vertical advection of the large-scale heat and moisture fields by compensating subsidence. The result is usually heating and drying (since $\partial \bar{s}/\partial p < 0$, $\partial \bar{q}/\partial p > 0$), although superadiabatic lapse rates in the traditional sense ($\partial s/\partial p > 0$) are also possible at lower levels (cf. Flasar 1987), leading to subsidence cooling instead.

The second term represents detrainment, i.e., mixing of cloud properties into the environment, at cloud top. The cumulus cloud always detrains with $s_c > \bar{s}$ and $\bar{q}_c > \bar{q}$, causing a local warming and moistening of the environment. (Overshooting can be accommodated in (11) and (12) by spreading the detrainment term out over a width greater than the layer thickness Δp.) The third term is the reevaporation of falling condensate, which always cools and moistens the large-scale environment.

We note that latent heating within the cumulus cloud itself ($L\bar{C}$ in (5)) appears nowhere in the final form of the energy and moisture equations (11) and (12). This happens because latent heat release acts only to maintain buoyancy in the cumulus cloud, as represented by (10). The effect of latent heating appears *indirectly* in (11) and (12) as compensating subsidence. It is this behavior which largely differentiates heating by cumulus clouds from that by large-scale stratiform clouds—the cumulus vertical heating profile is not identical to the profile of latent heat release within the cloud.

The subsidence and detrainment contributions to $\partial \bar{s}/\partial t$ and $\partial \bar{q}/\partial t$ can now be calcu-

lated from (11) and (12). However, lifting of the parcel also produces condensation at a rate $\bar{C}$ in each layer. If the condensate from each level falls into unsaturated air outside the cloud, some of it may evaporate. A proper treatment of the evaporation term $\bar{E}$ in (11) and (12) is beyond the scope of any GCM parameterization because of the complexity of cloud microphysics. To estimate its effects, we start at cloud top and allow the condensed water at that level to fall to the layer below. This condensate is then permitted to evaporate into a specified fraction f_e of the mass of the environment at that level. Setting $f_e = 0$ implies that all condensed water falls back through the saturated cloud updraft with no reevaporation. This absolute lower limit corresponds to the hypothesis of Lunine and Hunten (1987). It may be approached on Jupiter because assessments of Jovian water cloud microphysics suggest extremely efficient conversion of cloud water to precipitation (Carlson *et al.* 1988). In reality, wind shear tilts the updraft and causes some of the condensed water to fall through unsaturated surrounding air. For terrestrial deep cumulus, experience with the GISS GCM indicates that $f_e = 0.5 \ M_c\Delta t/\Delta p$, where Δt is the model timestep, gives a realistic relative humidity profile (Del Genio and Yao 1988). Since we expect the deeper Jovian clouds to be more efficient than their terrestrial counterparts, we perform computations for the terrestrial value of f_e and for $f_e = 0$ as upper and lower limits for reevaporation on Jupiter.

Reevaporation only occurs to the extent that the available fraction of the environment f_e is unsaturated. Any condensate remaining at the level below cloud top after this fraction saturates combines with condensate produced at this level and drops to the next layer, where the process is repeated. The total condensate left at the lower boundary of the model is the convective precipitation. The maximum amount of reevaporation $\Delta q = \bar{E}_{max}\Delta t$ in any layer is not simply $\bar{q}^* - \bar{q}$, because cooling is si-

multaneously occurring, lowering $\bar{q}^*$. A self-consistent first estimate of the degree of evaporation and cooling which leaves a layer just saturated can be obtained from the slope of the Clausius–Clapeyron equation. Let $\bar{T}_{old}$ and $\bar{T}_{new}$ be the temperature of the fraction f_e before and after evaporation, respectively. Taylor expanding $\bar{q}^*$, we get

$$\bar{q}^*(\bar{T}_{new}, p) \cong \bar{q}^*(\bar{T}_{old}, p)$$
$$+ \left(\frac{\partial \bar{q}^*}{\partial \bar{T}}\right)_{\bar{T}_{old}} (\bar{T}_{new} - \bar{T}_{old}). \quad (13)$$

Since the phase change takes place at constant p, $L\Delta q = L[\bar{q}^*(\bar{T}_{new}, p) - \bar{q}] = c_p(\bar{T}_{old} - \bar{T}_{new})$. Substituting this in (13), subtracting $\bar{q}$ from each side, and solving for Δq, we get

$$\Delta q = \bar{E}_{max}\Delta t$$
$$= \frac{\bar{q}^*(\bar{T}_{old}, p) - \bar{q}}{1 + (L/c_p)(\partial \bar{q}^*/\partial T)_{\bar{T}_{old}}}. \quad (14)$$

The actual evaporation into the layer fraction f_e is limited to the available condensate and may thus be less than $\bar{E}_{max}$. Because of the nonlinearity of the Clausius–Clapeyron equation, we iterate several times on (14) to derive an accurate saturated state. The evaporated condensate and associated cooling are then mixed into the environment following (11) and (12).

The same procedure is used to calculate the condensation rate $\bar{C}$ in the cloud updraft consistent with moist adiabatic ascent. Saturation in the updraft is measured with respect to ice ($L = 2.8 \times 10^6$ J kg^{-1}) rather than liquid water ($L = 2.5 \times 10^6$ J kg^{-1}) when $T_c < T_I$. We set $T_I = 0°C$ in most of our experiments. Sensitivity tests with $T_I = -40°C$ exhibit quantitative but not qualitative differences. Falling snow is assumed to melt at $0°C$; the resulting atmospheric cooling can be an important destabilizing influence.

Conrath and Gierasch (1984) and Gierasch et al. (1986) have concluded from an analysis of Voyager IRIS spectra that disequilibrium of the parahydrogen fraction (f_p) occurs in the middle and upper troposphere of Jupiter. They suggest that large-

scale vertical upwelling may account for the observations. Moist convection is another possible mechanism for the efficient transport of f_p. On the time scale of a convective event, ortho–para conversion can safely be neglected. The conservation equation for f_p analogous to (11) and (12) therefore takes the simple form

$$\frac{\partial \bar{f}_p}{\partial t} \cong -\tilde{M}\frac{\partial \bar{f}_p}{\partial p}$$
$$- (f_{pc} - \bar{f}_p)\frac{M_c}{\Delta p}\delta(p - p_\iota), \quad (15)$$

where f_{pc} is given by $\bar{f}_p$ at cloud base, which evolves with time. Subsidence increases f_p at depth, while detrainment injects air with low f_p at cloud top. Given sufficient time, this mixing would homogenize the vertical distribution of f_p. However, we will see that the dependence of moist convection on humidity at cloud base usually causes it to cease well before complete mixing is achieved.

We advect f_p as a passive, conserved tracer in our computations merely to deduce the characteristic signature of cumulus effects on the f_p distribution. On longer time scales, of course, ortho–para conversion is an important source term affecting the f_p balance. We have not included f_p-related differences between plume and environment adiabats or the feedback of changes in f_p on the adiabatic lapse rate, primarily because we wish to isolate moist convection effects with as few other complexities as possible. To the extent that ortho–para processes stabilize the lapse rate, they should act somewhat like entrainment in their effects on moist convection, lowering the cloud-top height by 50–100 mb (compare Figs. 5 and 8 in Stoker 1986). This effect is more important for water clouds on the cold outer planets than on Jupiter.

Besides moist convection, two other physical processes are included in the model. Dry convection (i.e., convection not dependent on latent heat release for its existence) is diagnosed whenever the verti-

cal structure is statically unstable. Traditionally this means a lapse rate steeper than the dry adiabat ($\partial \bar{s}/\partial p > 0$), but this ignores possible stabilization by molecular weight layering (cf. Flasar 1987). We assess static stability instead with respect to virtual dry static energy $\bar{s}_v = c_p \bar{T}_v + gz$. When $\partial \bar{s}_v/\partial p > 0$, a standard dry convective adjustment homogenizes s, q, and f_p between adjacent layers. This process is ubiquitous below cloud base and can also occur in isolated layers above cloud base because of destabilization by cumulus transports.

At the top of a dry convection layer, mixing of moisture may create supersaturation, causing a stratiform cloud to form (similar to marine stratocumulus which cap the Earth's planetary boundary layer). As a result, q will only be well-mixed in the lower parts of some dry convective layers and will follow the saturation curve in the upper parts. The terminology "dry" convection in this case refers only to the fact that it is static rather than conditional instability which occurs. Locally saturated conditions may also be produced by moist convective detrainment and reevaporation (e.g., anvil cirrus). In such cases we use (14) to maintain saturated conditions and rain out the excess in the same manner used to handle convective condensate.

The tests for moist and dry convection start at the lowest layer and proceed upward until the first unstable layer is found. The computations described above are performed and then the cycle is repeated at all higher potential cloud base layers (because cumulus can originate from perturbations at any level, not just the original LCL). Thus, more than one cumulus cloud and/or dry convection layer are possible in the same timestep. The only remaining issue is how to calculate M_c, the classical closure problem of cumulus parameterization which we explore in Sections 3 and 4.

A simple example illustrates the strong control that moist convection exerts on moisture profile of Earth's tropical troposphere. We initialize the terrestrial version of the model with observed temperatures above the 500-mb level, a dry adiabat below, and saturated humidity at all levels. These initial conditions are far removed from any physical state ever realized on Earth (but analogous to assumptions often made for Jupiter). We allow the cumulus parameterization, with an arbitrary specified M_c, to modify this initial state until it is neutrally stable to moist convection. $\bar{T}$ increases and $\bar{q}$ decreases below cloud top due to precipitation in this example because we include no evaporative source, such as an ocean, at the surface.

The resulting relative humidity ($\bar{q}/\bar{q}^*$) profile is plotted in Fig. 2, along with observations for the Intertropical Convergence Zone (Arakawa and Chen 1987). The model reproduces the observed humidity profile within the variability of the observations (10–15%) at all levels below the tropopause except near the surface. Excessive drying there can be removed by including a moisture source due to ocean evaporation, or by parameterizing saturated downdrafts in the model (Del Genio and Yao 1988). Thus, despite the complexity of cumulus dynamics and the imposition of an unrealistic initial state, the model nonetheless reproduces the salient features of the terrestrial water vapor distribution. This gives us confidence that the parameterization will yield plausible estimates for moist convection effects on Jupiter.

For Jupiter, our nominal model consists of 140 equally spaced (in p) layers with resolution $\Delta p \cong 50$ mb spanning the 10 mb to 7-bar range. We have also performed sensitivity tests with values of Δp ranging from 25 to 700 mb. The chosen resolution affects the calculations in two subtle ways. Subsidence is assumed to advect air over a depth Δp (i.e., to the next lowest level) for each convective event, while the updraft itself penetrates over a pressure range $p_b - p_t$. The ratio $\Delta p/(p_b - p_t)$ thus gives the relative areas of active updrafts and the subsiding environment. If a fraction f_c of the mass of a layer rises in a given event, then, $\sigma =$
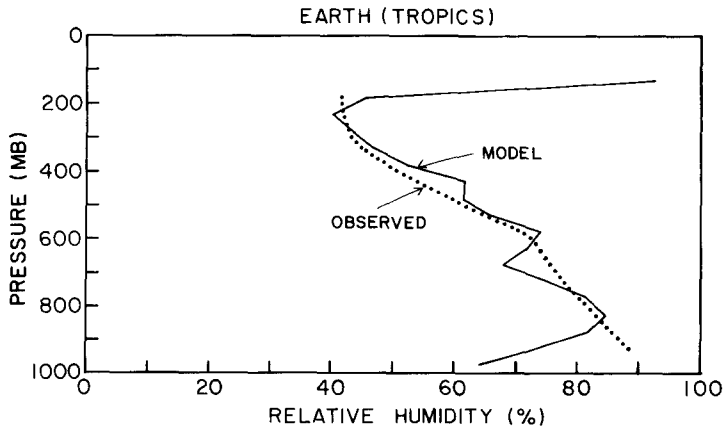
FIG. 2. Solid line. The relative humidity ($\bar{q}/\bar{q}^*$) profile for the neutrally stable moist convective state produced by the terrestrial version of the cumulus parameterization when initialized with observed temperatures above 500 mb, a dry adiabat below, and saturated water vapor mixing ratio at all levels Dotted line· Observations for the Atlantic ITCZ adapted from Arakawa and Chen (1987).

$f_c \Delta p/(p_b - p_t)$. Typical values are $f_c \cong .02$ and $p_b - p_t \cong 4.65$ bar for a deep Jovian cumulus in our model, giving $\sigma \cong 2 \times 10^{-4}$. This easily satisfies the parameterizability constraint $\sigma \ll 1$ discussed earlier and falls in the midrange of values considered by Lunine and Hunten (1987). A second effect of resolution concerns the onset of convection. We test for convection by lifting a cloud-base parcel one layer to mimic the effect of random small-scale perturbations. The thicker the layers, the greater the implied instantaneous lifting and therefore the more likely it is that parcels will be raised to their LFC. This affects the results quantitatively but not qualitatively. In the presence of a computed or prescribed upward $\bar{\omega}$ due to dynamics on larger scales, this becomes a moot point because the large-scale upwelling ultimately brings a parcel to its LFC regardless of layer thickness.

We initialize the model with the nominal Jovian temperature profile of Conrath and Gierasch (1984) for $p \leq 800$ mb. For $p > 800$ mb, we assume a virtual dry adiabat with fixed c_p/R and consider small perturbations about this lapse rate for individual experiments. The initial water vapor mixing ratio is assumed constant at a given deep abundance value up to the LCL and is set to the local saturation value above. Parahydrogen fraction is initialized to be in equilibrium; the values are taken from Massie and Hunten (1982). The values of all physical constants for Jupiter used in the calculations are taken from Allison and Travis (1986).

3. NEUTRALLY STABLE MOIST CONVECTIVE STATES

The central problem of cumulus parameterization is the determination of the cumulus mass flux M_c. A number of approaches exist, none of which has been judged superior by consensus (cf. Frank 1983). Indeed, completely different closure assumptions can give very similar results in a terrestrial GCM (Yao and Del Genio 1989). Since we have no observational basis for constraining ideas about Jovian moist convection, we consider two extreme views about how convection might operate on Jupiter.

In the first scenario we imagine that the atmosphere of Jupiter is weakly forced, so that moist convection dominates all other physical processes. (An alternative scenario is discussed in Section 4.) A saturated, dry adiabatic state cannot be maintained under these conditions because it is unstable to moist convection. If convection

is the dominant process, it will relax the initial state to a configuration which is just neutrally stable with respect to cumulus clouds. In this limit, internal heating, large-scale motions, and radiation act only to force moist convection but have no direct influence on the realized vertical structure. This philosophy has been used in recent studies of terrestrial hurricanes (Rotunno and Emanuel 1987). The concept is similar to that of lapse rate adjustment in one-dimensional radiative–convective models, but with both temperature and moisture structure calculated explicitly using the penetrative cumulus model.

With this assumption M_c can be specified arbitrarily, because there are no other time constants in the problem. The larger the value used for a single convective event, the faster the model relaxes to neutral stability. The final state is essentially independent of the value used as long as it is not so large as to overstabilize the atmosphere. For our computations we used $M_c = .05\Delta p$ per convective event, a typical value for the terrestrial tropics. However, we also tested values from .01 to .1 to verify that the answer is independent of this parameter.

The resulting vertical structure is sensitive to the assumed initial deep abundance of water, the efficiency of condensate reevaporation, and the static stability of the initial temperature profile. The detailed distributions of reevaporation and dry convective mixing vary with small changes in lapse rate. We therefore perturbed the initial virtual dry adiabat by small amounts (from 0 to $\pm 10^{-1}$°K integrated over the depth of the fluid below 800 mb) and averaged the results over 10 such realizations. All the experiments we conducted fall into one of three general regimes.

a. Moist Convective Regime

This behavior occurs when $\chi \lesssim \chi_s$ at depth in the initial state (where $\chi_s = 9.97 \times 10^{-3}$ is the water mass mixing ratio for solar abundance of oxygen), condensate reevaporation is neglected ($f_e = 0$) or very small,

and the initial lapse rate is slightly subadiabatic as judged by $\partial \bar{s}_v / \partial p$. In this regime, dry convection is limited to levels below the LCL, while transports above the LCL are due solely to cumulus. For our canonical example, we select $\chi = \chi_s$ and $f_e = 0$; this is the Lunine and Hunten (1987) scenario. The resulting vertical structure is shown in Fig. 3, with s and s_v converted to potential temperature θ and virtual potential temperature θ_v (defined by analogy to (3)) for ease of interpretation.

For solar abundance the LCL is at 5.0 bars. Moist convection starts at this level and above, and the deepest events penetrate to 335 mb. Because $\bar{q}^*$ decreases with height above the LCL, significant molecular weight layering is present in the initial profile. Thus, θ decreases with height while θ_v is effectively constant below 800 mb (cf. Flasar 1987). The final profile of θ_v (Fig. 3a) shows only a hint (<0.1°K) of a stable layer directly above cloud base. A large increase in stability, on the other hand, has taken place at 800–1400 mb, just beneath the stable upper troposphere.

The degree of stabilization at cloud base is much less than the theoretical value for complete latent heat release and molecular weight layering. Ignoring condensate loading for simplicity, this value can be written (cf. Gierasch and Conrath 1985) as

$$\Delta \theta_v^{\max} \cong \chi \left(\frac{L}{c_p} + \theta \right). \qquad (16)$$

At cloud base, $\Delta \theta_v^{\max} \cong 4.9$°K for $\chi = \chi_s$. There are several reasons why the maximum is not realized. The most important is subsidence, which advects stable air downward from the base of the upper troposphere but can only advect air with $\partial \theta_v / \partial p \cong 0$ near cloud base. Detrainment injects warm air only at cloud top, reinforcing the effect of subsidence. With $f_e = 0$, there is no evaporative cooling at lower levels to produce a jump in stability. The net result is that the effect of the latent heat release is felt almost completely at cloud top. Subsi-
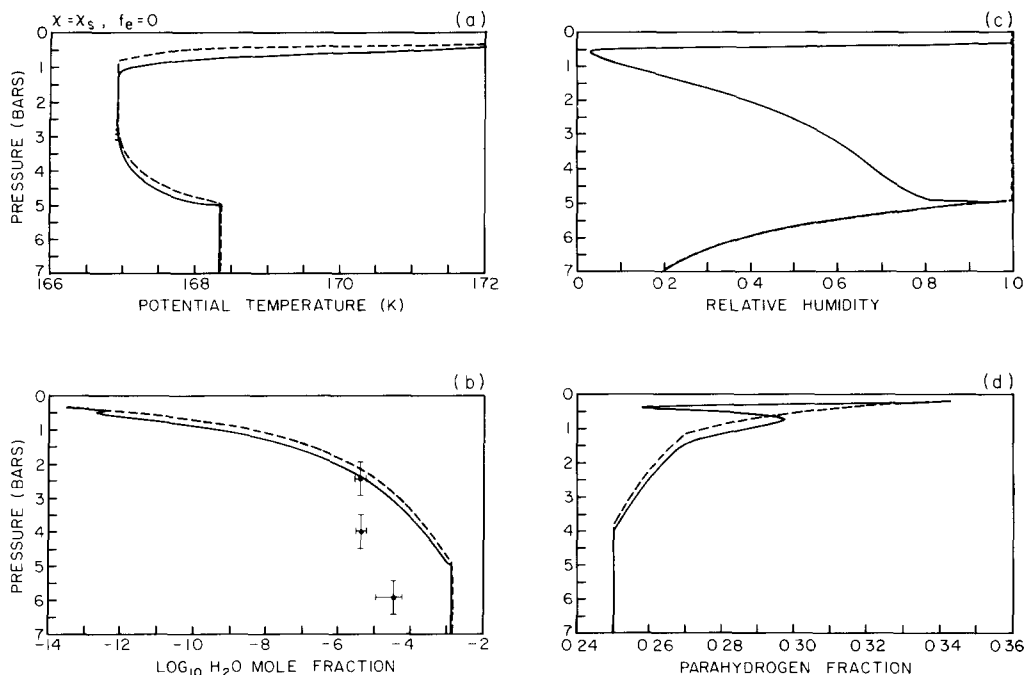
FIG. 3. Initial (dashed) and final (solid) profiles of (a) potential temperature, (b) H_2O mole fraction, (c) relative humidity and, (d) parahydrogen fraction for the neutrally stable moist convective calculations for $\chi = \chi_s$, $f_e = 0$, and a slightly statically stable initial profile. The dotted line in (a) represents the final profile of virtual potential temperature; the initial profile of θ_v below the 800-mb level is approximately a straight line, coincident with θ at $p = 2$ bars. The H_2O mole fractions at 2, 4, and 6 bars inferred by Bjoraker et al. (1986) are indicated for comparison in (b)

dence drying slightly reduces molecular weight layering, but this is offset by small changes in θ.

The initial and final molar mixing ratio profiles are shown in Fig. 3b, along with the values retrieved by Bjoraker et al. (1986). Subsidence effectively shifts the entire moisture profile downward by about 200 mb over most of the depth of cumulus events, while detrainment maintains saturation locally near cloud top. The effect of subsidence does not penetrate further downward because subsidence is very slow relative to the convection itself, according to (7), and because only a small fraction of the mass of the environment is displaced in each event. The final temperature profile is conditionally unstable but moist convectively neutral to small displacements, because moist convection also requires sufficiently high rela-

tive humidity at cloud base to enable such displacements to lift air to its LCL and LFC. As subsidence dries out the cloud-base environment, it eventually stabilizes the atmosphere by making it too dry for further cumulus activity. This combination of a steep lapse rate with insufficient low-level moisture also partly explains why moist convection occupies such a small fraction of the terrestrial tropics at any instant.

Locally, especially just below cloud top, relative humidities below 5% are possible (Fig. 3c). Drying is greater at upper levels because a given subsidence displacement Δp traverses a greater distance Δz at lower pressures. Qualitatively similar behavior occurs on Earth (Fig. 2). At deeper levels, relative humidity steadily increases. The nominal model mixing ratios exceed those

of Bjoraker *et al.* by a factor of 50 at the 4- and 6-bar levels. The coarse resolution results are somewhat drier but never within an order of magnitude of Bjoraker *et al.* Thus, while the mechanism of Lunine and Hunten operates in the model, it cannot sustain itself long enough to produce severe drying over a deep layer. We emphasize that this result was obtained under the most favorable circumstances possible, i.e., with no condensate evaporation and no other dynamical processes mixing water upward from depth. We conclude that a deep solar abundance of water is incompatible with the results of Bjoraker *et al.* if moist convection is the controlling process.

The initial and final parahydrogen profiles for this case are presented in Fig. 3d. Detrainment at cumulus cloud tops deposits high-temperature equilibrium hydrogen near visible cloud levels, creating an f_p minimum there. Below cloud top, subsidence increases f_p above its local equilibrium value. The resulting vertical gradient of f_p is negative from 385 to 734 mb. The final state is not well-mixed because drying at cloud base shuts off convection before the mixing can be completed. It is interesting to note that Gierasch *et al.* (1986) retrieved f_p profiles with negative gradients at several latitudes near the equator at slightly higher levels in the upper troposphere. Cumulus detrainment appears to be the only plausible explanation for these negative gradients. If so, f_p profiles may be a useful diagnostic for locations of deep cumulus convection on Jupiter.

Comparison of this experiment with the results of Bjoraker *et al.* (1986) might lead one to conclude that water must be depleted globally by substantial amounts. This interpretation, however, cannot be reconciled with the effects of moist convection either. Figure 4 shows the mixing ratio profile produced by cumulus activity when we set $f_e = 0$ and $\chi = .02\chi_s$, selected to approximately match the Bjoraker *et al.* value at 6 bars. With this little water vapor in the atmosphere, the LCL is much higher (2.8 bars) and cloud tops are lower (784 mb). Below 2.8 bars, the mixing ratio is constant because only dry convection operates—there are no processes capable of differentiating water vapor at these levels. This is clearly inconsistent with the Bjoraker *et al.* profile, which implies an order of magnitude increase in mixing ratio between 4 and 6 bars. Thus, the vertical structure deduced by Bjoraker *et al.* cannot be explained by either a solar or depleted deep water abundance if convection determines the local mixing ratio.
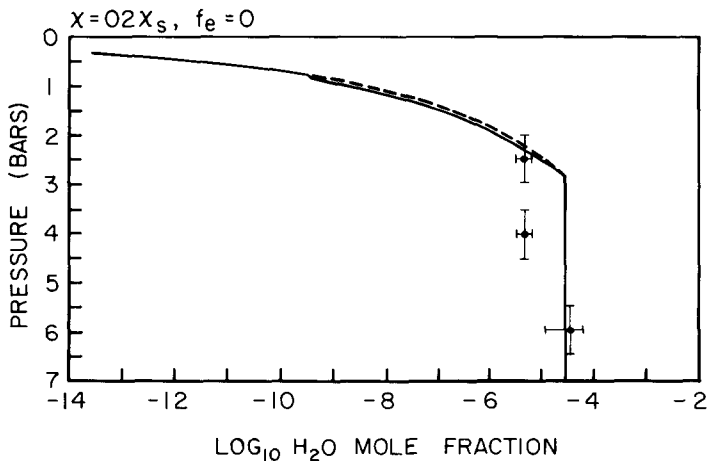

FIG. 4. As in Fig. 3b, but for $\chi = .02\chi_s$.

b. Mixed Moist–Dry Convective Regime

Microphysical processes such as condensate evaporation and melting of snow can be a destabilizing influence on the small scale on Jupiter. In the preceding examples, the former effect was ignored and the latter occurred only at cloud base or below because the LCL is at 0°C in our model for solar water abundance. As a result, moist convection exists in isolation above the LCL in these cases, and the environment is generally free of water clouds other than the cumulus clouds themselves for $p > p_t$.

In other cases, though, it is possible for cooling and/or molecular weight differentiation by microphysical processes to overcome the stabilizing tendency of cumulus subsidence and generate local dry convection layers even though the initial θ_v profile is statically stable. This occurs when the water abundance is supersolar, even with no condensate evaporation, and for solar abundance if reevaporation is sufficiently strong. In this situation, moist and dry con-

vection coexist above the LCL, with the former forcing the latter.

An example of this mixed regime ($\chi = 2\chi_s, f_e = 0$) is shown in Fig. 5. Initially, only moist convection exists, with cloud bases as deep as 5.5 bars and cloud tops as high as 285 mb. Falling snow melts at 5.0 bars, above cloud base, creating a local minimum in $\bar{\theta}_v$ there. Dry convection layers set in first at this level, and then above, while cumulus clouds continue to be forced. The locations of these dry convection regions are best seen as layers of constant f_p (Fig. 5d). Negative f_p gradients also exist near cloud top in this case (335–534 mb), but are smaller in magnitude because of episodic dry mixing events.

The lower parts of these well-mixed layers are also fairly well-mixed in water vapor (Fig. 5b). The upper parts saturate at times, though, forming multiple layers of large-scale cloud. This is easily seen in the relative humidity profile (Fig. 5c) as transitions from dry air to air with ≥90% relative humidity in the large-scale mean (implying
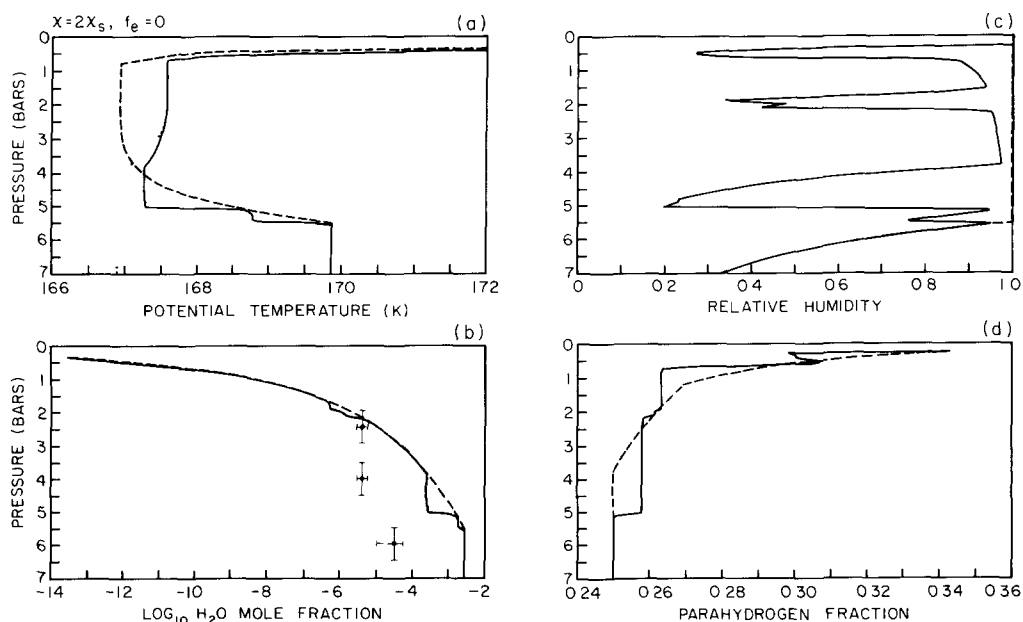

FIG. 5. As in Fig. 3, but for $\chi = 2\chi_s$.

large fractional cloud cover). Such transitions occur from about 5 to 2 bars and again from 2 bars to 600 mb. The precise number and location of these layers is undoubtedly sensitive to details of the temperature profile and cloud microphysics. However, experiments with $\chi = 3\chi_s$ and $5\chi_s$ give basically the same configuration. The upward mixing of moisture by dry convection makes it even harder to produce a uniformly depleted water vapor profile. The θ_v profile (Fig. 5a) now contains a substantial stable layer ($\Delta\theta_v \cong 0.7°K$) over roughly a scale height above cloud base. This is still <10% the maximum value obtained from (16), but large enough to maintain a thermal wind of almost 10 m sec^{-1} if translated into a belt-zone temperature difference. The existence of this stable layer is directly attributable to the presence of dry convection layers with capping stratus clouds, which localize latent heat effects to the altitudes at which the latent heat is released.

Figure 6 shows another example of the mixed regime, this time for $\chi = \chi_s$ and f_e set to the terrestrial value. Dry convection lay-

ers exist in this case also, but they are forced by the cooling and moistening effects of condensate reevaporation. The combination of evaporation and dry convection produces a more complicated relative humidity profile with a number of potential layers of partial cloud cover (Fig. 6c). The agreement with Bjoraker $et\ al.$ is predictably worse (Fig. 6b). A stable layer with $\Delta\theta_v \cong 0.4°K$ (Fig. 6a), much stronger than that which exists without evaporation (Fig. 3a), is produced. In general, the profiles for this case resemble those for higher water abundance. However, when $f_e \neq 0$, the final θ_v profile can be sensitive to changes in resolution or small changes in static stability. It is possible, for example, to produce a strong stable layer ($\Delta\theta_v \cong \Delta\theta_v^{max}$) that extends from cloud base to the upper troposphere with no intervening neutrally stable region.

The dependence of $\Delta\theta_v$ on χ in the nominal model is not linear, and is qualitatively different for different f_e. Without evaporation, there is a sharp increase in $\Delta\theta_v$ at the transition from the pure moist convective
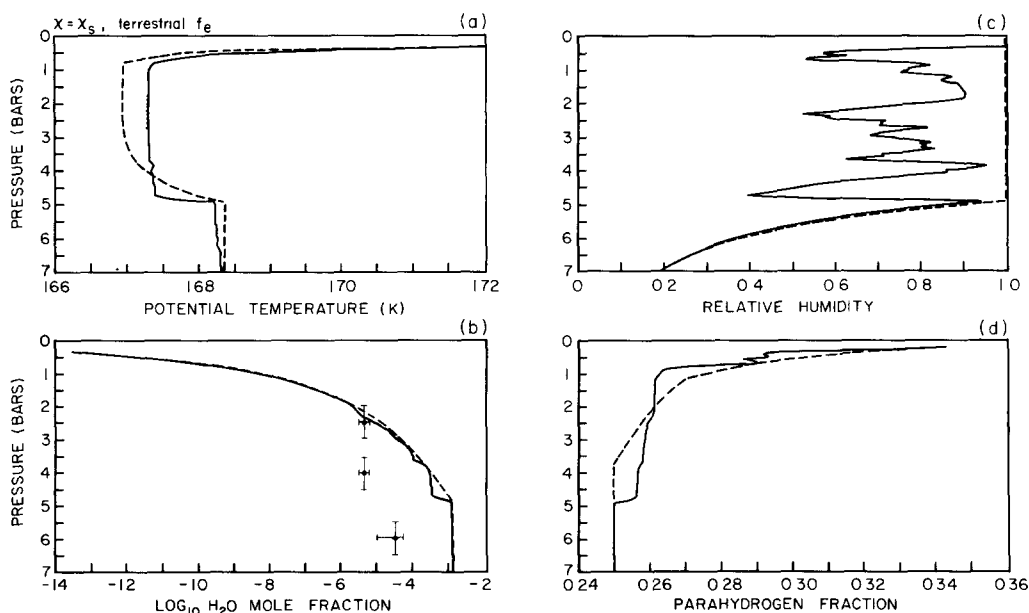

FIG. 6. As in Fig. 3, but for terrestrial f_e.

regime to the mixed regime ($\chi \cong \chi_s$). For higher χ, the behavior is irregular, but in general $\Delta\theta_v$ slightly declines up to $\chi = 5\chi_s$. With evaporation, $\Delta\theta_v$ increases steadily with χ. In all cases, though, $\Delta\theta_v/\Delta\theta_v^{max} \lesssim 0.1$. These results apply only to isolated stable layers between 2 and 5 bars; we assess the effect of convection on the total static stability below 800 mb in Section 5.

c. Dry Convective Regime

Thus far we have discussed only cases in which the initial θ_v profile was slightly statically stable. When the initial state is sufficiently close to the dry virtual adiabat (i.e., when the θ_v difference between 800 mb and 7 bars is $\leq 10^{-2}$°K), small isolated dry convective events begin to disrupt the pure moist convective regime but do not qualitatively change the vertical structure. When the initial state is superadiabatic, though, a completely different regime emerges, one dominated by dry rather than moist convection.

An example of this dry convective regime ($\chi = \chi_s$, $f_e = 0$) is shown in Fig. 7.

Initially, the entire atmosphere below 800 mb dry convectively adjusts in response to the superadiabaticity. Moist convection is inhibited in this region. The only cumulus clouds which occur are shallow ones which originate near 800 mb and lose buoyancy at 435 mb. Latent heat release at the top of the dry convective layer forces a secondary dry convection episode down to 2.4 bars.

The result is a stable layer about 0.6 scale heights thick with magnitude $\Delta\theta_v \cong 1.4$°K $\cong 0.3\Delta\theta_v^{max}$ (Fig. 7a). $\Delta\theta_v$ increases with χ in this regime, although not quite linearly (e.g., $\Delta\theta_v \cong 4$°K for $\chi = 5\chi_s$). The moisture profile exhibits a single dry layer near the base of the secondary dry convection region with saturated or nearly saturated conditions above and below down to the LCL (Figs. 7b, 7c). The position of the LCL itself shifts upward from 5 to 4.3 bars because water has been rained out of the column. The f_p distribution (Fig. 7d) contains two well-mixed layers marking the primary and secondary dry convection regions, and effectively no regions with negative gradients. This latter feature may be
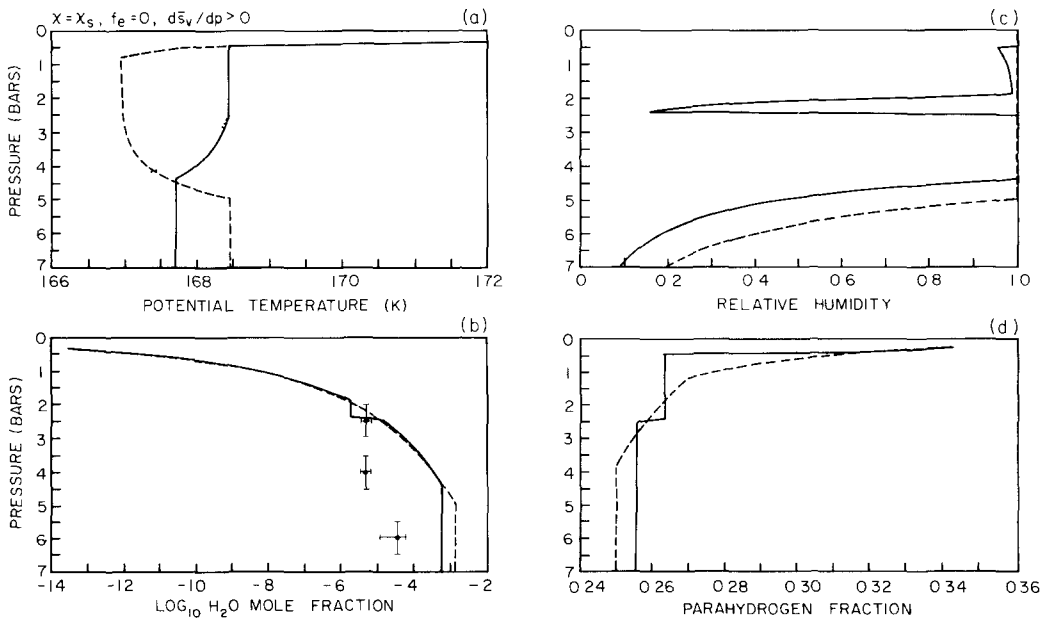

FIG. 7. As in Fig 3, but for a slightly statically unstable initial θ_v profile

useful in distinguishing the effects of dry and moist convection in observations which deduce f_p distributions. The shallow cumulus region and the second dry convection layer disappear when $\chi \lesssim .05\chi_s$. Otherwise, the simulations in this regime are quite insensitive to variations in abundance and the efficiency of condensate evaporation.

4. A QUASIEQUILIBRIUM CONVECTIVE STATE

A completely different scenario for moist convection effects on Jupiter can arise if we simultaneously consider other physical processes. Arakawa and Schubert (1974), for example, have postulated that terrestrial cumulus clouds stabilize the environment at about the same rate as large-scale processes (advection, radiation, surface fluxes) destabilize it. Such a "quasiequilibrium" between the cumulus scale and the large scale seems to be typical of most tropical regions (Lord and Arakawa 1980, Arakawa and Chen 1987). The resulting vertical structure can be different from that produced when cumulus processes acting alone drive the atmosphere to convective neutrality.

Radiative processes can presumably be ignored over most of the altitude range of Jovian H_2O cumulus clouds. The primary constraint is the Jovian internal heat flux $F_i = 5.4$ W m^{-2} which is continuously destabilizing the atmosphere near the LCL. The first step in constructing a Jovian quasiequilibrium state is thus to estimate the cumulus mass flux whose sensible and latent heat flux is just sufficient to carry the internal heat flux from cloud base to cloud top.

For simplicity, we ignore condensate evaporation and melting in the calculation of M_c under the assumption that these processes are feedbacks resulting from the convection well after its onset. Thus, subsidence from the layer above is the only effect of cumulus at cloud base ($p = p_b$) in the early stages of an event. Assuming

$\bar{\omega}(p_b) = 0$, (7) gives $\bar{M} = -M_c$. The internal flux converges in a layer Δp at the deepest p_b; this contributes to the total eddy flux convergence in (5). If this heat is removed by moist convection, then in a time Δt,

$$\frac{\Delta \bar{h}}{\Delta t} = \frac{\Delta \bar{s}}{\Delta t} + L\frac{\Delta \bar{q}}{\Delta t} \cong M_c\left(\frac{\Delta \bar{s}}{\Delta p} + L\frac{\Delta \bar{q}}{\Delta p}\right)$$
$$= -g\frac{F_i}{\Delta p}, \quad (17)$$

using (1), (2), (11), and (12). Solving (17) for M_c, we get

$$M_c = -\frac{gF_i}{\Delta \bar{s} + L\Delta \bar{q}}. \quad (18)$$

For cumulus events which originate at levels above the deepest cloud base, we use an analogous formula with the internal heating replaced by the heating due to prior cumulus events from deeper levels. To maintain equilibrium, a similar amount of heat is simply removed at cloud top ($p = p_t$) to crudely mimic the effects of radiation and unspecified dynamical transports in the upper troposphere.

For $p_b > p > p_t$, however, equilibrium may not exist in this configuration because of unbalanced convective heating and stratiform latent heating. Even at cloud base, subsequent evaporation and/or melting of condensate can disrupt the equilibrium. In three dimensions, horizontal variations in cumulus activity will exist, and associated with these will be pressure gradients, convergence, and large-scale vertical motion. A one-dimensional model is incapable of predicting large-scale motions; our intention here is only to illustrate one possible interaction between the cumulus scale and the large scale. As a first approximation we merely calculate the vertical velocity at each level that is required to just balance the convective and stratiform heating from the previous timestep. The horizontal convergence pattern which gives this vertical motion field is implicit. In the well-mixed region below the LCL, we extrapolate the vertical velocity linearly in p to zero at 7 bars.

The simultaneous operation of all these processes in the model allows a quasiequilibrium state to develop. Since moist convection is no longer operating in isolation, we must choose a timestep for integration in order to predict from (18) the fraction of mass of a layer which rises per event. In the terrestrial GCM, $\Delta t = 1$ hr, which is longer than the time scale of individual cumulus. For our Jovian cumulus, which are of order 100 km in depth, the same Δt can be justified if the mean updraft speed is $\gtrsim 25$–30 m sec^{-1}. This is more vigorous than typical terrestrial cumulus updrafts but less than the limiting updraft speed for Jovian cumulus deduced by Stoker (1986). A timestep of 1 hr is also comparable to estimates of the time required for precipitation to form in a Jovian water cloud (Carlson et al. 1988). To conserve heat and moisture during the integration, we allow all precipitated water to reevaporate and mix uniformly throughout the unsaturated region below the original LCL, even when $f_e = 0$ above.

The nominal model ($\chi = \chi_s$, $f_e = 0$) was run for 1000 hr, which is sufficient time for more than 10 complete overturnings due to subsidence. The model reaches its quasiequilibrium state in 50–100 hr. When the initial θ_v profile is statically unstable, the resulting quasiequilibrium state resembles that for the dry convective regime discussed earlier (Fig. 7) above the LCL. Below the LCL, where we deposit all precipitation in this scenario, significant moistening and cooling occur, giving $\Delta\theta_v = 3.9°$K in the 2–5 bar region. This large $\Delta\theta_v$ is an artifact of the model's lower boundary being at 7 bars; with a deeper model, dry convection would mix much of this cool, moist subcloud air to deeper levels and produce a weaker stable layer at cloud base.

When the initial profile is statically stable enough to prevent dry convective mixing from top to bottom, a different result emerges (Fig. 8). A series of thin dry-convection layers of variable depth, coexisting initially with a single mode of deep
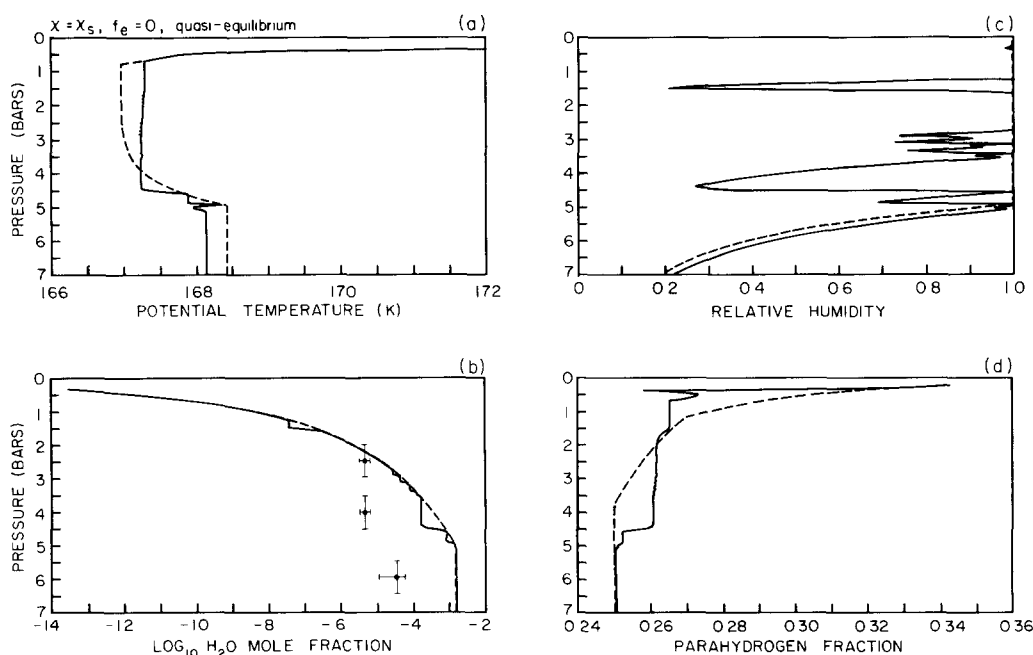

FIG. 8. As in Fig 3, but for the quasiequilibrium experiment with $\chi = \chi_s$, $f_e = 0$, and an initial θ_v profile statically stable by $10^{-3}°$K between 800 mb and 7 bars.

moist convection originating at 4.6 bars and later with only shallow cumulus near 5 bars, represents the quasiequilibrium structure. This layered structure is most similar to that of the mixed moist–dry regime discussed earlier. The thin convection layers are well-mixed in θ and f_p but the jumps between layers are small, of order 10^{-3} K and $10^{-4\circ}$, respectively (Figs. 8a, 8d). The structure is easier to see in the mixture profile (Fig. 8b, 8c). The layers tend to saturate near their upper boundary, producing a multilayer structure of thin stratiform cloud. The number and thickness of layers varies with vertical resolution and the degree of stability of the basic state, but the tendency for thin layers is present to some extent in all cases.

The required vertical velocity field, averaged over the last 500 hr, is shown in Fig. 9a. At most levels, equilibrium is achieved rapidly and no large-scale vertical motion is needed after an initial adjustment. The ve-

locities are largest and most persistent within the thin convection layers, and small or near zero at the interfaces. There is no large-scale vertical structure in the velocity field. Vertical velocity slowly decreases with time; by the end of the integration, vertical motion was absent within most of the layers. In real atmospheres, there may be a lag time between convection and large-scale vertical motion (cf. Lindzen and Nigam 1987). To the extent that this occurs, a true equilibrium will not exist, and vertical motions on larger scales will always be present.

When condensate evaporation is permitted above cloud base, the atmosphere evolves differently. Thin convection layers are still present but are not as well-mixed in moisture. Potential temperature, rather than decreasing with height above cloud base, now increases by 0.2°K between 5.0 and 4.5 bars and then decreases from there to 2.5 bars by a similar amount. Since evaporation is neglected in the derivation of (18), our parameterized moist convection cannot by itself maintain an equilibrium state. A vertical motion field thus develops, primarily in response to evaporative cooling (Fig. 9b). The vertical velocity in this case has significant large-scale vertical structure because evaporation extends over depths much larger than a single thin convection layer. The pattern of alternate upwelling and downwelling is controlled by the sign of $\partial\bar{\theta}/\partial p$ and the necessity for adiabatic warming to compensate evaporative cooling. Similar physics produces mesoscale downdrafts beneath the anvils of tropical cloud clusters on Earth (Zipser 1977). The rising motion above 1 bar is an exception; it reflects large-scale adiabatic cooling in response to cumulus detrainment and subsidence in the stable upper troposphere. This is more analogous to the forcing of the rising branch of the Hadley circulation in the ITCZ on Earth.

The vertical profiles of potential temperature, moisture, and parahydrogen fraction are reminiscent of the "staircase" structure
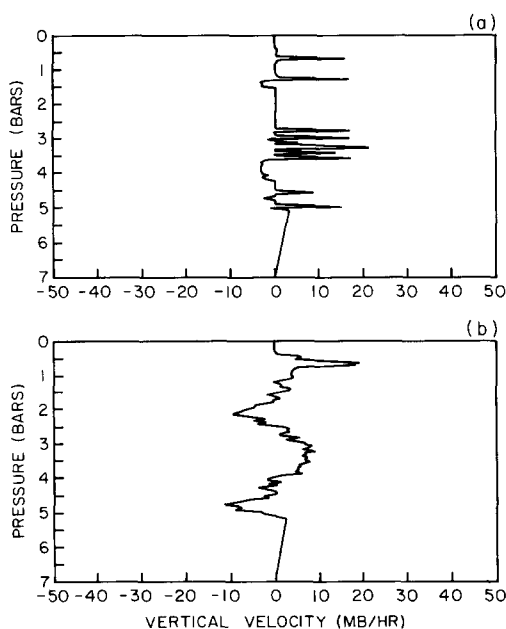

FIG 9. The mean vertical velocity $(-\bar{\omega})$ profile (positive upward) for the last 500 hr of (a) the quasiequilibrium experiment of Fig. 8, and (b) a similar experiment but with terrestrial f_e.

which occurs in certain double-diffusive convection situations (Turner 1973). Gierasch and Conrath (1987) have predicted that such a structure must exist on Uranus to reconcile the peculiar features of Voyager temperature and f_p retrievals for that planet. The staircase phenomenon is well-known in oceanography, where temperature and salt produce opposing effects on buoyancy. In Jovian atmospheres, molecular weight differentiation by condensing species plays a role analogous to salt in the ocean.

The mechanism which gives rise to thin layered convection in our model is not completely clear. In the oceanic case, as in the proposal of Gierasch and Conrath, the different molecular diffusivities of heat and salt (or moisture) are responsible. In our simulation, however, there is no explicit diffusion. Hints of thin layering exist even when large-scale vertical advection is not included in the model, but the layered structure is intensified by the predicted vertical motions. Likewise, a cumulus mass flux greater than that predicted by (18), which forces a stronger vertical velocity field, produces a more obvious staircase pattern. This suggests that mixing by cumulus subsidence and large-scale motions may act to some extent like diffusion in the model. The requirement for thin layers is that the more rapidly diffusing component be unstably stratified. Define vertical length scales for heat and moisture variations $H_\theta = \bar{\theta}(\partial\bar{\theta}/\partial z)^{-1}$ and $H_q = \bar{q}(\partial\bar{q}/\partial z)^{-1}$, respectively. Then the effective "diffusivities" of heat and moisture caused by cumulus and large-scale motions with velocity W are $\kappa_\theta = WH_\theta$ and $\kappa_q = WH_q$. Since $H_\theta > H_q$, $\kappa_\theta > \kappa_q$; this is precisely what we need, since heat is unstably stratified ($\partial\bar{\theta}/\partial p > 0$) above the LCL.

The alternative to thin layers in double-diffusive convection is deep columns which are thin in the horizontal, a phenomenon called "salt fingers" by oceanographers (Turner 1973). These occur when the more rapidly diffusing component is stably strati-

fied. This type of stratification is not relevant in the mean on Jupiter. However, in the vicinity of Jovian cumulus clouds, where warm, moist air is being detrained at cloud top, and in rainshafts, where precipitation loading is an important effect on buoyancy, severe moist downdrafts and perhaps local dry updraft columns may develop by analogy with the ocean. This point has been raised by Stoker et al. (1988) in the Uranus case.

Finally, we note the implications of our results for moist convection on the other giant planets. Since M_c is directly proportional to F_i in (18), we expect somewhat less vigorous moist convection on Saturn. For Neptune and Uranus, whose internal heat fluxes are one and two orders of magnitude smaller than Jupiter's, respectively, very weak, sporadic cumulus activity may be sufficient to carry the internal flux to the emission level unless the deep thermal structure on these planets is quite different from that on Jupiter. In the absence of strong drying by cumulus subsidence, condensibles such as water and methane should be present at generally high environmental relative humidities on Uranus and Neptune (Del Genio 1989).

5. DISCUSSION AND CONCLUSIONS

The foregoing results are intended only as illustrations of the possible large-scale ramifications of moist convection on Jupiter. The near-neutral stability of Jovian atmospheres, which ensures a complex interplay between dry and moist convection, makes detailed prediction for Jupiter more uncertain than for Earth. Different convective regimes may exist at different locations and times, but our relatively crude representation of convection and the absence of true dynamic or radiative feedbacks in our one-dimensional model precludes investigation of such regime transitions. Explicit representation of dry convective fluxes is one possible improvement. Since cloud microphysics clearly influences our results,

combination of this model with a detailed microphysical model would also be fruitful. Extension of the model to deal with ortho–para effects on dry and moist convective stability is an obvious next step, and probably a necessary one for application to Uranus and Neptune. Inclusion of downdraft effects, as in the terrestrial version of the model, may be especially important for the deep atmosphere. Nonetheless, some general conclusions about the vertical structure of Jupiter's atmosphere are unavoidable; these are discussed below.

a. Water Abundance and Cloud Structure

Regardless of the abundance at depth, we cannot reconcile the severely depleted water vapor profile deduced by Bjoraker *et al.* (1986) with the effects of moist convection. There are four reasons for this: (1) In the absence of other processes, cumulus subsidence near cloud base will stabilize the atmosphere against further cumulus activity well before the drying effects of subsidence aloft can penetrate through large depths; (2) Microphysical processes tend to stimulate local dry convection episodes which rapidly mix moisture upward; (3) If condensate evaporation occurs above cloud base, e.g., from mesoscale anvils or tilted updrafts, direct moistening of the environment will result; (4) Large-scale vertical motions will advect moisture upward at some times and places when moist convection is not in instantaneous equilibrium with other physical processes.

We see only two possible ways to resolve this discrepancy. If cloud opacity is significantly greater in regions of large-scale upwelling than in regions of downwelling, the airborne 5-μm observations may be weighted heavily toward relatively clear areas with large-scale sinking motion. If we simply prescribe a strong constant downward velocity in our model, rather than calculating vertical motion interactively, both cumulus and stratiform water clouds are suppressed and a uniformly dessicated vertical profile of water vapor is produced.

Any such vertical motion persisting on a large scale would not be colocated with significant deep moist convection. This explanation seems unlikely in view of the fact that Bjoraker *et al.* (1986) find only a factor of 4 difference between the water mixing ratio inferred for NEB hot spots, presumably among the clearest regions on Jupiter, and other areas in the Voyager IRIS data. However, this does not preclude the presence of substantial horizontal variations of humidity associated with large-scale convergence/divergence patterns.

The other possibility is that the mixing ratios inferred from the 5-μm data are assigned to deeper pressure levels than is appropriate. Carlson *et al.* (1990), for example, show that the retrieved water abundance and its vertical profile are quite sensitive to the assumed temperature profile and the vertical distribution and radiative properties of clouds. Their analysis of the same Voyager data suggests solar or supersolar water abundance instead. We emphasize that the Bjoraker *et al.* water profile cannot plausibly be interpreted in terms of globally depleted water. The order of magnitude increase in H_2O mole fraction between 4 and 6 bars that they infer would occur well below the LCL in this case, and no obvious water differentiation process exists at depth.

A final comment concerns the common assumption that a massive water cloud should exist on Jupiter if water is not depleted. In the presence of moist convection, a massive water cloud originating at the water LCL would not be expected. In the terrestrial tropics, deep optically thick cumulus occupy a very small fractional area, and upper troposphere cirrus is the dominant cloud type. This point is discussed by Weidenschilling and Lewis (1973) and Ingersoll (1976). In our model, a complex multilayer water cloud structure is possible, and by analogy to Earth, likely. The relationship between the vertical cloud structure and the global water abundance may therefore not be straightforward.

b. Static Stability

Table I shows the change in $\delta\theta_v = \theta_v(800$ mb$) - \theta_v(\text{LCL})$ and $\delta\theta$ (defined similarly) that occurred between the beginning and end of each of our quasiequilibrium experiments. Since $\delta\theta_v \cong 0$ in the initial state, the numbers in the first column represent the maximum effective buoyancy contrast available to drive large-scale motions in this layer. The numbers in the second column indicate the degree of stability that convection would produce if it affected only the temperature field. The difference between the changes in $\delta\theta$ and $\delta\theta_v$ is a measure of changes in molecular weight layering.

The static stability caused by moist convection is seen to be due entirely to latent heat release. Drying at cloud base actually reduces molecular weight layering—the change in $\delta\theta_v$ is smaller than that in $\delta\theta$. Molecular weight layering present in the initial profiles just offsets a negative initial $\delta\theta$. Thus, virtual effects, although an integral part of cumulus convection on Jupiter, are not enhanced by convection. Stabilization increases with increasing water abundance, increasing importance of dry over moist convection, and at times with increasing efficiency of condensate evaporation. The microphysical effects are not simple; their behavior is sensitive to both the

abundance of water and the cumulus closure assumption. However, in all experiments the final static stability is considerably less than the maximum value (16).

These considerations have several implications for Jovian dynamics. The buoyancy contrasts implied by Table I are sufficient to give rise to large thermal wind shears, but not enough to completely explain the magnitude of zonal jets at the visible cloud level unless (perhaps) water is considerably enriched. For solar abundance, static stability increases as condensate evaporation becomes more important. On the other hand, rainfall evaporation is favored in cloud clusters by strong vertical wind shear. Thus, an interesting positive feedback between large-scale motions and microphysical processes is possible.

Since large static stability is favored in our experiments by a dominance of dry over moist convection, we might speculate that the magnitude of observed jets is a tracer of the strength of cumulus activity. The strong 23°N jet, for example, would be a region of relatively weak moist convection. We have not considered cumulus momentum transport in this paper, but detrainment of low-momentum air at cloud top in regions of active cumulus would reinforce this effect.

Our results indicate that an isolated stable layer at depth, with an intervening neutrally stable layer above, is possible when condensate evaporation and dry convection above cloud base are important. We cannot, however, rule out the possibility of a stable layer which extends all the way from cloud base to the upper troposphere. When isolated stable layers occur, their thickness is always less than or comparable to a scale height. This occurs because stratiform cloud formation localizes latent heat release to a moisture scale height, which is much less than a pressure scale height. The same argument in reverse applies to evaporative cooling. Our results are consistent with the conditions required by Allison (1990) for trapping of equatorial waves, but

TABLE I

A COMPARISON OF THE FINAL MINUS INITIAL VERTICAL CONTRASTS IN θ_v AND θ BETWEEN 800 mb AND THE LCL FOR EACH QUASIEQUILIBRIUM EXPERIMENT

Experiment	Change (°K) in	
	$\delta\theta_v$	$\delta\theta$
$\chi = \chi_s, f_e = 0, \partial\bar{s}_v/\partial p < 0$	0 30	0.38
$\chi = 2\chi_s, f_e = 0, \partial\bar{s}_v/\partial p < 0$	0.80	1.05
$\chi = 3\chi_s, f_e = 0, \partial\bar{s}_v/\partial p < 0$	1 29	1.85
$\chi = \chi_s,$ terrestrial $f_e, \partial\bar{s}_v/\partial p < 0$	1 08	1 33
$\chi = 2\chi_s,$ terrestrial $f_e, \partial\bar{s}_v/\partial p < 0$	0.80	1.06
$\chi = \chi_s, f_e = 0, \partial\bar{s}_v/\partial p > 0$	1.37	2.20
$\chi = 2\chi_s, f_e = 0, \partial\bar{s}_v/\partial p > 0$	2.22	4.09

Note The sign of $\partial\bar{s}_v/\partial p$ refers to the initial profile.

probably only if water is substantially enriched.

The foregoing remarks on static stability are valid only if the large-scale environment is sufficiently subsaturated so that dynamical displacements do not reach the LCL. In a saturated environment, virtual equivalent potential temperature is a more relevant indicator of stability, and the effective stability is likely to be much smaller.

c. Parahydrogen Fraction

The retrieval of f_p and its vertical gradient from Voyager IRIS data is notoriously uncertain (Conrath and Gierasch 1984, Gierasch et al. 1986). However, real global and regional variations appear to exist, and given the striking modifications of the f_p profiles in our model, it is useful to speculate about the role of convection in producing observed f_p variations.

Moist convection produces several characteristic signatures in f_p in the upper troposphere: (1) A local minimum at cloud top generally in the range 0.26–0.30, well below the local equilibrium value; (2) A negative vertical gradient in the subsidence region just below cloud top; (3) Positive gradients above and sometimes just below these regions. When dry convection dominates at upper levels, the f_p values are generally slightly higher than when cumulus control the structure, and the vertical gradient is near zero.

If the results of Gierasch et al. (1986) are taken at face value, some tentative interpretations follow. A concentration of cumulus activity at low latitudes might contribute to the low values of f_p there (Stoker 1986) and the few instances of negative f_p gradients they observe. (The IRIS data refer to a level generally slightly higher than our cloud tops, but moderate overshooting can reconcile this.) This does not conflict with the Gierasch et al. proposal of a slow planetary-scale circulation with equatorial upwelling. In fact, a similar circulation at depth, providing moisture convergence at cloud base and adiabatic cooling aloft,

would be needed to continuously supply moisture for such a Jovian version of the ITCZ. Bjoraker et al. (1986) note that the equatorial region exhibits large variability in 5-μm emission, which is consistent with episodic, localized deep convection and accompanying cirrus. Coffeen's (1974) analysis of Pioneer 10 Imaging Photopolarimeter data shows higher cloud tops near and just north of the equator than anywhere else on Jupiter except the Great Red Spot; this is also consistent with vigorous low-latitude moist convection.

The equatorial plumes near 9°N latitude are often cited as possible evidence of deep cumulus convection on Jupiter (cf. Hunt et al. 1981). Retrieved values of f_p are higher there than at the equator, while the vertical gradient is sharply positive (Gierasch et al. 1986). If we assume that the plumes are the centers of the most vigorous moist convection to be found on Jupiter, with substantial overshooting (cf. Stoker 1986), the cloud tops might penetrate above the 270-mb level of the IRIS observations. We might then observe the subsidence region below the detrainment level; this could account for the observed f_p behavior. West et al. (1985) found no correlation of f_p with the anvil region well downstream from the plume head, but f_p need not be anomalously low there if we are not viewing the detrainment altitude.

Finally, we note that f_p is relatively large, and its vertical gradient near zero, in the vicinity of the 23°N jet. This is consistent with our earlier suggestion of weak cumulus activity, and perhaps local dry convective mixing, at this latitude.

It is hoped that the Galileo probe will address some of the outstanding questions about water and its role on Jupiter. A direct estimate from the mass spectrometer and an indirect retrieval from the net flux radiometer may be possible if the abundance is sufficiently high. The deep stable layers we obtain in some experiments have a static stability of only 10^{-1}°K km^{-1}; combined with uncertainties in the correct dry adiabat

due to ortho–para processes, it seems un-
likely that such stable layers can be de-
tected. However, such a layer would be in-
dicated indirectly by the presence of a
complex multilayer water cloud structure,
deduced by the nephelometer and net flux
radiometer experiments. The Galileo probe
is targeted for entry at the latitude of the
equatorial plumes. While this is potentially
exciting for aficionados of moist convec-
tion, it should be kept in mind that the
probe results are likely not to be typical of
conditions elsewhere on Jupiter. Mapping
of cloud top heights by the Galileo orbiter
photopolarimeter radiometer may provide a
useful large-scale context for interpreting
the probe data in terms of the presence or
absence of moist convection on Jupiter.

REFERENCES

ALLISON M. 1990. Planetary waves in Jupiter's equa-
torial atmosphere. *Icarus,* **83,** 282–307

ALLISON, M., AND L D TRAVIS 1986. Astronomical,
physical, and meteorological parameters for plane-
tary atmospheres In *The Jovian Atmospheres*
(M Allison and L D. Travis, Eds), pp 293–319
NASA CP-2441, Washington, D C.

ARAKAWA, A., AND J.-M CHEN 1987 Closure as-
sumptions in the cumulus parameterization prob-
lem. *J Meteor. Soc Japan,* special issue on Short-
and Medium-Range Numerical Weather Prediction,
107–131.

ARAKAWA, A., AND W H. SCHUBERT 1974 Interac-
tion of a cumulus cloud ensemble with the large-
scale environment. Part I. *J Atmos Sci* **31,** 674–
701.

BARCILON, A., AND P GIERASCH 1970. A moist, Had-
ley cell model for Jupiter's cloud bands *J Atmos
Sci.* **27,** 550–560

BJORAKER, G L., H P LARSON, AND V G KUNDE
1986. The abundance and distribution of water va-
por in Jupiter's atmosphere *Astrophys. J.* **311,**
1058–1072

CARLSON, B. E., M. J PRATHER, AND W B. ROSSOW
1987 Cloud chemistry on Jupiter *Astrophys J.* **322,**
559–572

CARLSON, B. E , W. B. ROSSOW, AND G. S. ORTON
1988. Cloud microphysics of the giant planets. *J
Atmos. Sci.* **45,** 2066–2081.

CARLSON, B. E., A. A. LACIS, AND W. B. ROSSOW
1990. The abundance and distribution of water va-
por in the Jovian troposphere as inferred from Voy-
ager IRIS observations. *Icarus,* in preparation.

COFFEEN, D. L 1974. Optical polarization measure-
ments of the Jupiter atmosphere at 103° phase angle.
J. Geophys Res **79,** 3645–3652

CONRATH, B. J., AND P. J. GIERASCH 1984. Global
variation of the para hydrogen fraction in Jupiter's
atmosphere and implications for dynamics on the
outer planets *Icarus* **57,** 184–204.

DEL GENIO, A. D 1989. Moist convection in the atmo-
spheres of Uranus and Neptune *Bull. Amer As-
tron. Soc* **21,** 917–918

DEL GENIO, A D , AND M.-S YAO 1988. Sensitivity
of a global climate model to the specification of con-
vective updraft and downdraft mass fluxes. *J. At-
mos Sci.* **45,** 2641–2668

FEGLEY, B , JR., AND R. G. PRINN 1988 Chemical
constraints on the water and total oxygen abun-
dance in the deep atmosphere of Jupiter *Astrophys.
J.* **324,** 621–625

FLASAR, F. M 1987 Cumulus dynamics in hydrogen
atmospheres *Bull. Amer. Astron Soc* **19,** 829.

FRANK, W. M. 1983 The cumulus parameterization
problem *Mon Weather Rev* **111,** 1859–1871

FU, R , A. D DEL GENIO, AND W B ROSSOW 1990
Deep convective clouds in the tropical Pacific ob-
served from ISCCP radiances *J. Climate,* in
press.

GIERASCH, P. J 1976 Jovian meteorology Large-
scale moist convection *Icarus* **29,** 445–454

GIERASCH, P J , AND B J. CONRATH 1985. Energy
conversion processes in the outer planets. In *Recent
Advances in Planetary Meterology* (G. Hunt, Ed),
pp. 121–146 Cambridge Univ Press, Cambridge.

GIERASCH, P J , B J CONRATH, AND J A
MAGALHAES 1986. Zonal mean properties of Jupi-
ter's upper troposphere from Voyager infrared ob-
servations *Icarus* **67,** 456–483

GIERASCH, P. J., AND B J CONRATH 1987 Vertical
temperature gradients on Uranus. Implications for
layered convection *J. Geophys Res.* **92,** 15,019–
15,029

HANSEN, J., G. RUSSELL, D. RIND, P STONE,
A. LACIS, S LEBEDEFF, R RUEDY, AND L TRAVIS
1983 Efficient three-dimensional global models for
climate studies: Models I and II. *Mon Weather
Rev* **111,** 609–662

HUNT, G. E , B J CONRATH, AND J. A. PIRRAGLIA
1981 Visible and infrared observations of Jovian
plumes during the Voyager encounter *J Geophys
Res.* **86,** 8777–8781.

INGERSOLL, A. P. 1976 The atmosphere of Jupiter
Space Sci. Rev. **18,** 603–639.

KNUPP, K R., AND W R COTTON 1985 Convective
cloud downdraft structure An interpretive survey.
Rev Geophys. **23,** 183–215

LELLOUCH, E., P DROSSART, AND T. ENCRENAZ 1989. A new analysis of the Jovian 5-μm Voyager/ IRIS spectra. *Icarus* **77**, 457–465.

LINDZEN, R S., AND S. NIGAM 1987 On the role of sea surface temperature gradients in forcing low-level winds and convergence in the tropics *J Atmos. Sci.* **44**, 2418–2436

LORD, S J., AND A. ARAKAWA 1980 Interaction of a cumulus cloud ensemble with the large-scale environment. Part II. *J Atmos Sci.* **37**, 2677–2692

LUNINE, J. I., AND D M. HUNTEN 1987. Moist convection and the abundance of water in the troposphere of Jupiter. *Icarus* **69**, 566–570.

MANABE, S., J. SMAGORINSKY, AND R. F. STRICKLER 1965 Simulated climatology of a general circulation model with a hydrological cycle *Mon Wea. Rev* **93**, 769–798.

MASSIE, S. T., AND D. M HUNTEN 1982. Conversion of para and ortho hydrogen in the Jovian planets *Icarus* **49**, 213–226

RIEHL, H., AND J S. MALKUS 1958 On the heat balance in the equatorial trough zone *Geophysica* **6**, 503–538.

ROTUNNO, R , AND K A. EMANUEL 1987. An air–sea interaction theory for tropical cyclones. Part II. Evolutionary study using a nonhydrostatic axisymmetric numerical model. *J Atmos. Sci.* **44**, 542–561.

SAUNDERS, P M. 1957. The thermodynamics of saturated air: A contribution to the classical theory *Q J. R. Meteor. Soc* **83**, 342–350.

STOKER, C. R 1986. Moist convection. A mechanism for producing the vertical structure of the Jovian equatorial plumes. *Icarus* **67**, 106–125.

STOKER, C R , D. M KING, R E. YOUNG, AND O. B. TOON 1988. Theoretical modeling studies of moist convection on Uranus. *Bull. Amer. Astron. Soc* **20**, 822.

TURNER, J S. 1973. *Buoyancy Effects in Fluids*. Cambridge Univ Press, New York.

WEIDENSCHILLING, S. J , AND J W. LEWIS 1973. Atmospheric and cloud structures of the Jovian planets. *Icarus* **20**, 465–476.

WEST, R. A., P. N. KUPFERMAN, AND H. H HART 1985. Voyager 1 imaging and IRIS observations of Jovian methane absorption and thermal emission Implications for the cloud structure. *Icarus* **61**, 311–342

YAO, M.-S., AND A. D DEL GENIO 1989. Effects of cumulus entrainment and multiple cloud types on a January global climate model simulation *J. Climate* **2**, 850–863.

ZIPSER, E. J 1977. Mesoscale and convective-scale downdrafts as distinct components of squall-line circulation. *Mon. Wea. Rev.* **105**, 1568–1589.